Weakening thickness dependence of critical current density in $YBa_2Cu_3O_{7-x}$ films using nanotube pore insertion

Xiang Wang,* Alan Dibos, and J. Z. Wu
Department of Physics and Astronomy, University of Kansas, Lawrence, Kansas 66045, USA
(Received 22 January 2008; revised manuscript received 1 April 2008; published 29 April 2008)

$YBa_2Cu_3O_{7-x}$ films with nanotube pores (YBCO/NTPs) aligned along normal of the film have been fabricated with thickness ranging from 0.1 to 1.2 μm. When compared to YBCO films without NTPs, YBCO/NTP samples show much reduced thickness dependence of the critical current density J_c, in addition to the overall higher J_c values, in magnetic fields below the matching field of the NTPs. These results suggest that the through-thickness NTPs may provide an enhanced pinning force per vortex length (F_p) which remains a constant at various thicknesses.

DOI: 10.1103/PhysRevB.77.144525 PACS number(s): 74.25.Sv, 74.25.Qt, 74.62.Dh, 61.46.Fg

The monotonic reduction in critical current density J_c with increasing thickness (t) in high T_c superconductor (HTS) films has been one of the major roadblocks for commercialization of high T_c superconductor coated conductors (HTSCCs)—the so-called second generation HTS wires.[1] At 77 K and self-field (SF), the J_c of $YBa_2Cu_3O_{7-x}$ (YBCO) films typically decreases by 50%–60% when the film thickness increases from 0.2 to about 1 μm. While misoriented grains as well as degraded epitaxy may be responsible for the J_c reduction at larger $t>0.6$ μm, such microstructure deterioration in thinner films, where the major J_c reduction up to 40% occurs, is usually insignificant.[2–4] This raises a question on the mechanism responsible for the J_c-t behavior. Interestingly, most observed J_c-t data at 77 K and SF fall on top of the $J_c \propto t^{-1/2}$ curve.[5] Considering J_c can be expressed as $J_c = cF_p/\Phi_0$ in the critical state model, where F_p is the pinning force per vortex length, Φ_0 is the flux quanta, and c is the speed of light, the $J_c \propto t^{-1/2}$ curve implies a thickness dependence of $F_p \propto t^{-1/2}$. Such a behavior has been predicted in the collective pinning (CP) model under the assumption that each vortex is collectively pinned by surrounding weak point defects.[6] According to this model, F_p follows $F_p \propto t^{-1/2}$ as long as t is much less than the longitudinal pinning correlation length (Larkin length) L_c. However, L_c is sensitively determined by the property of pinning centers. Weak point pins such as oxygen vacancies only yield L_c of several nanometers,[7] which is far below the thickness range where J_c-t occurs in HTS films. For strong pinning systems, such as YBCO thin films with a high density of strong point pinning centers like secondary phase inclusions,[8,9] the original CP model has been modified based on the consideration of multiscale pinning structure. An extremely long L_c up to ~ 1 μm, which covers the thickness range where the t dependence of J_c occurs, is anticipated due to the suppressed local vortex bending in YBCO thin films.[5]

Our recent study of the J_c-t behavior in pulsed laser deposited YBCO films suggests that the modified CP model indeed applies, despite the complication caused by thermally assisted flux motion (TAFM), in a wide range of temperature (T) from 10 to 88 K and a magnetic field (H) up to 5 T.[10,11] This result also supports the argument that large randomly distributed point defects, such as secondary phase inclusions and precipitates, are most likely the dominant pinning centers in typical YBCO films.[9] A question follows on what kinds of defect structures may allow elimination of the J_c-t in HTSCC by maintaining a constant F_p at variable thickness.

One strategy to achieve a pseudothickness-independent F_p is to construct multilayered YBCO films, in which a thick YBCO film is evenly divided into n layers by $n-1$ thin insulating layers such as CeO_2.[12,13] In a recent experiment, we studied J_c as a function of the CeO_2 layer thickness (t_I) in YBCO/CeO_2/YBCO trilayers while the thickness of each YBCO layer was fixed at 0.25 μm.[12] Interestingly, the J_c in the trilayer samples monotonically increases with t_I until it saturates at about 1.3 times of the J_c of 0.5-μm-thick single-layer YBCO film when t_I reaches to about 20 nm. A conductive atomic force microscopy study of the CeO_2 layer showed that an almost complete coverage of the underneath YBCO surface by CeO_2 layer occurs at $t_I \sim 20$ nm. This result suggests, although other arguments also exist,[13] that the CeO_2 spacers may simply decouple a long vortex into n short segments. Therefore, each vortex segment is capable of adjusting itself to accommodate the surrounding pinning centers without energy-costing bending. Consequently, the thin film J_c (or the J_c of the constituent YBCO layer) can be obtained in thicker films.[12] Nevertheless, the multilayer strategy technically involves a more complicated multitarget deposition, in addition to the capped J_c dictated by the constituent YBCO layer.

An ultimate solution of the J_c-t problem is to overpowering the point pins with strong aligned linear pins along the film thickness. These linear defects could provide not only a thickness independent but also enhanced F_p,[14] therefore optimized J_c in thick HTS films. This is, by all means, not an easy task since most reported impurity insertions in YBCO result in degraded J_c at SF and low H fields.[15] However, such degradation may not be an issue in nanotube pore (NTP) insertion. In this work, we show that aligned NTPs can be generated by using a nanoscale strain modulation method. This method has two important components, vicinal substrate and nanoparticle (NP) insertion, for controlling mechanical strain on the YBCO lattice at nanoscales. The NPs may be inserted either near the film and/or substrate interface or during the YBCO film growth. The local tune of the strain by the inserted NPs over the globally strained YBCO lattice on vicinal substrates plays a critical role in pore nucleation,

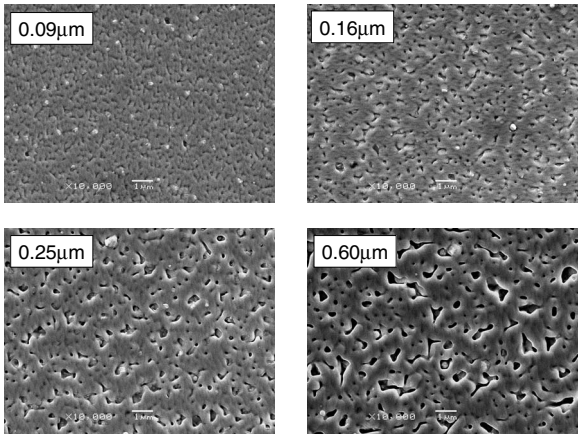

FIG. 1. SEM images of YBCO/NTP films at various thicknesses.

as evidenced from the initiation of pores directly atop the NPs.[16] A large number of NTPs of dimension from few to hundreds of nanometers uniformly form via self-assembly growth. No degradation occurs to T_c in these samples and the resistivity in longitudinal direction (along *ab* plane) is comparable to that of the typical YBCO films without impurity insertion.[17] In this work, we report the experimental results on a comparative study of J_c-t behavior between YBCO films with and without inserted NTPs.

Two sets of YBCO films with (YBCO/NTP) and without NTPs (standard YBCO film) were fabricated by using pulsed laser deposition (PLD) technique under similar growth conditions. The YBCO/NTP films were grown on 20° vicinal single crystal (001) $SrTiO_3$ substrates, while the standard YBCO films on single crystal (100) $LaAlO_3$ substrates. The laser energy density on the target was $\sim 3.2\ \mathrm{J/cm^2}$ and the repetition rate was 10 Hz. The deposition was carried out onto substrates heated to 765–775 °C in 230 mTorr oxygen partial pressure followed by annealing in 360 Torr oxygen for 50 min. In this experiment, although the film thickness ranges from 0.09 to 1.2 μm, the samples selected for the J_c-t study that have thickness of only up to 0.6 μm to avoid complication of the microstructure degradation in thicker films. After fabrication, silver contact pads were immediately deposited on to the films to minimize the surface resistance. For electrical transport measurement, a 20×400 μm bridge was patterned by using standard photolithography procedure. For YBCO/NTP films, the bridges were parallel to the longitudinal direction, constraining current only in the *ab* plane. *I-V* curves were measured by using the standard four-point configuration and a criterion of 1 μV/cm was applied to determine the J_c.

Figure 1 shows the scanning electron microscopy (SEM) images of four YBCO/NTP films with various thicknesses ranging from 0.09 to 0.6 μm. At $t=0.09$ μm, many pores are already formed in addition to some NPs on the surface. These NPs, which are mostly Y_2O_3 precipitates naturally occurred during the PLD process, serve as the seeds for NTPs to initiate. This means that the densities of NPs and pores are closely correlated.[16] With increasing t, the densities of both NP and pore dramatically decrease and at $t=0.16$ μm, only few NPs are observed and the pore density also drops to about 50% from $9-10/\mu\mathrm{m}^2$ to $4-5/\mu\mathrm{m}^2$. At $t=0.16$ μm, the visible pores have dimension typically about 100–200 nm. It should be mentioned that the pores with smaller dimension are not clearly visible at the magnification used while their presence was confirmed in transmission electron microscopy studies (not shown in this paper). With further increasing thickness, the pore density remains almost unchanged at around $4-5/\mu\mathrm{m}^2$ and some large pores of dimension on the order of 500–1000 nm appear as shown on 0.6-μm-thick sample.

In order to understand how pores evolve through the film thickness, a 1.2-μm-thick YBCO/NTP film was thinned via nine consecutive steps using ion milling and analyzed using SEM after each step of 0.12 μm thinning. Marks were employed so that the same pores can be monitored through the milling steps. Figure 2 includes the SEM images taken on the original sample surface ($R0$) and on each of the nine steps of milling ($R1-R9$). Many pores can be traced through different layers of the film and most of them are almost through the entire (for example, the three pores labeled, respectively, with cyan ovals, blue circles, and pink squares) or a large portion (green diamonds for a pore through the bottom half

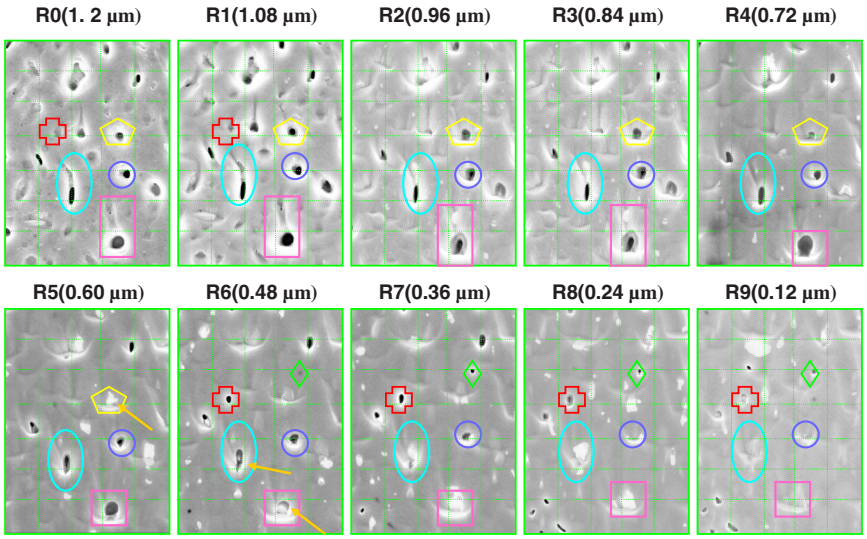

FIG. 2. (Color online) SEM images of a 1.2-μm-thick YBCO/NTP film at different stages of thinning using ion milling. $R0$ (1.2 μm) represents the original film and $Rn(d)$ represents the film after nth milling with remaining thickness d. The 500×500 nm^2 grids are applied to each image and a colored pattern is used for tracking a specific NTP through different layers of thickness.

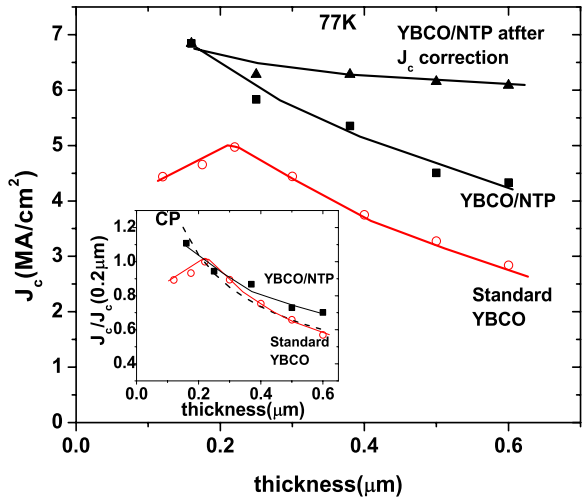

FIG. 3. (Color online) J_c-t curves of YBCO standard films (circles) and YBCO/NTP films (squares) at 77 K and SF. Also shown is the J_c-t curve of YBCO/NTP (triangles) assuming a thickness-independent NTP lateral dimension. The inset shows the J_c-t curves of the two types of films in a normalized scale J_c/J_c (0.2 μm). The same symbols as in Fig. 1 are employed for the two curves in the inset. The dash line indicates the fitting of the CP model.

of the film and yellow pentagons for a pore through the top half) of the film thickness. This means that they have nanotube geometry. We have also observed some pores closed at certain thickness and reappear (red crosses). Y_2O_3 NPs, which were confirmed with energy-dispersive x-ray spectroscopy, are visible at the bottom of NTPs (a few marked with yellow arrows), confirming that NPs indeed play a critical role in nucleation of the NTPs. It should be noted that the density of the Y_2O_3 NPs is at least an order of magnitude smaller than that near the film and/or substrate interface.[17] Above t=100 nm, the NP density is on the order of $0.2-0.3/\mu m^2$. In the thickness range from 0.16 to 0.6 μm, the density of the pore in YBCO/NTP films is more or less a constant, which agrees with Fig. 1. This suggests that the number of generated NTPs is comparable to that of disappeared NTPs in this thickness range, while the majority NTPs initiate at smaller thickness. Interestingly, most NTPs appear at the same or close to the same lateral location at different thicknesses while their lateral dimension experiences some increases through the 1.2 μm film thickness. This means that they are more or less straight nanotubes aligned along the normal of the film.

In Fig. 3, the J_c at SF and 77 K is plotted as a function of thickness for both YBCO/NTP (squares) and standard (circles) samples. Considering the possible nonuniformity of NTPs in the YBCO/NTP sample at smaller thickness, only the J_c of the films with thickness in the range of (0.16–0.6)-μm-thick film are included. The solid lines are guides for the eyes. There are two interesting observations in Fig. 3. First, the J_c values of the YBCO/NTP films are overall higher than that of the standard YBCO films in the same thickness range. At t=0.25 μm, the J_c of the YBCO/NTP sample is 5.83 MA/cm^2, which is ~20.7% higher than that of the standard YBCO sample, and at t=0.6 μm, it is ~52.8%. Note that the J_c values of the standard YBCO samples are between 5.0 and 2.8 MA/cm^2 at 0.2 $\mu m \leq t \leq 0.6$ μm, which are comparable to the typical J_c's around 5.5–3.5 MA/cm^2 reported in the same thickness range.[3,15] On the other hand, the YBCO/NTP films experience weaker thickness dependence of J_c than the standard ones do. This latter observation can be further illustrated in the inset of Fig. 3 by replotting the two curves in Fig. 3 on a normalized scale J_c/J_c (0.2 μm). With increasing t from 0.25 to 0.6 μm, for example, J_c drops only 26% for the YBCO/NTP films as opposed to a 40% reduction in the standard YBCO films. Moreover, the J_c-t of the standard YBCO films can be well fitted by $J_c \propto t^{-1/2}$ as predicted by modified CP model in most of the thickness range except the deviation below 0.2 μm. This deviation, which leads to a switch from increasing J_c to decreasing J_c with increasing t, has been previously observed.[9,10,18] In our previous paper, we argued that this deviation from $J_c \propto t^{-1/2}$ is most probably related to the pronounced TAFM, since a shorter vortex collectively pinned by point defects is more easily thermally activated than a longer one within L_c.[10] In contrast to the standard films, such switch is not observed in the according thickness range for YBCO/NTP, suggesting that the TAFM is greatly suppressed as point defect pinning is overpowered by NTP pinning.

Although a weaker thickness dependence of J_c is observed in the YBCO/NTP samples, the remaining J_c-t is unexpected if NTP dominates the pinning. A possible explanation is the reduced cross-sectional area owing to those enlarged NTPs at larger thickness, which leads to an underestimated J_c in thick films. To quantify this argument, the NTPs' lateral dimension increase, which translates to reduction in the cross-sectional area for the electrical current, was estimated based on the SEM images shown in Fig. 1. When t increases from 0.16 to 0.25 μm, the reduced current cross-sectional area is about 7%. It increases to ~29% when t is increased to 0.6 μm. Considering the correction of the cross-sectional area, an "ideal" J_c-t curve is extracted and added in Fig. 3 (triangles). It is not surprising that the J_c-t curve of YBCO/NTP films with perfectly straight NTPs drops only ~5% as thickness increases from ~0.25 to 0.6 μm. This greatly weakened J_c-t clearly demonstrates that NTP insertion is indeed an effective approach to eliminate J_c-t by providing a thickness independent F_p. In addition, the ideal NTP's lateral dimension should be on the order of coherent length in ab plane ξ_{ab} (~3.5 nm for YBCO at 77 K).[14,19] Higher J_c values are anticipated in YBCO/NTP films if the lateral dimension of the NTP could be reduced to few nanometers close to ξ_{ab}.

Based on the observed NTP's density in Fig. 1, the matching field H_m is estimated to be about 8–10 mT. The actual H_m may be slightly higher due to those uncounted smaller NTPs in few to tens of nanometer regime. As the applied magnetic field H exceeds H_m, some vortices will no longer be pinned by the NTPs. Instead, they will be pinned by other weaker pinning centers. With increasing H, the NTP will gradually render the dominancy to those weaker pinning centers. These weaker pinning centers are most likely isotropic ones such as secondary phase inclusions. Consequently, the CP-type J_c-t curves observed in the standard YBCO samples will be resumed in YBCO/NTP samples at a certain $H \gg H_m$.

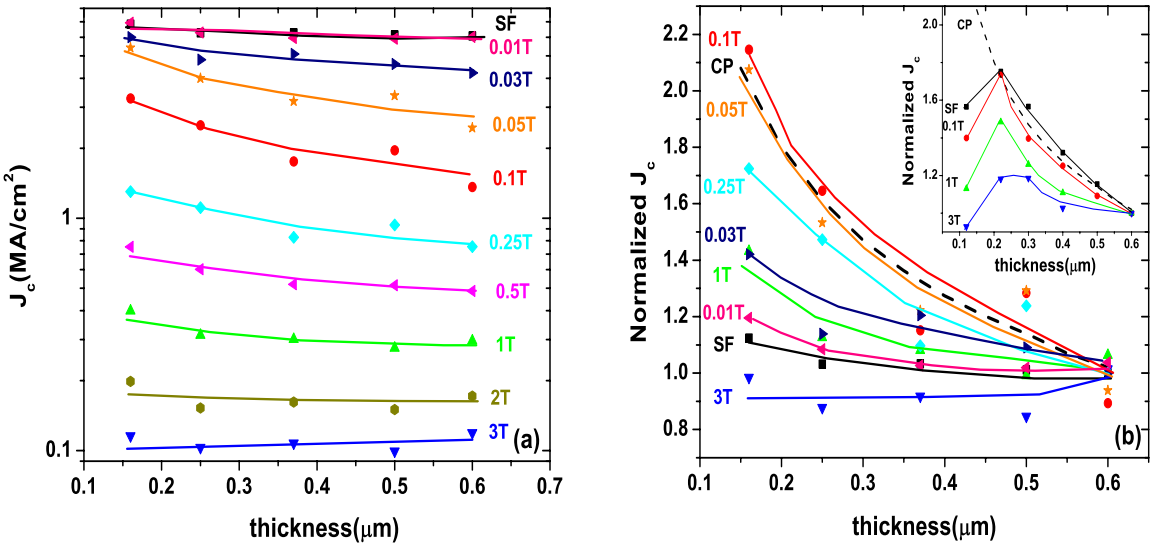

FIG. 4. (Color online) (a) J_c-t curves of YBCO/NTP films at 77 K and various H fields. Solid lines are drawn to guide the eyes; (b) J_c-t of YBCO/NTP and standard YBCO films (inset) at 77 K and various H in a normalized scale J_c/J_c (0.6 μm). The dash line indicates the fitting of the CP model.

This argument seems to agree well with the enhanced thickness dependence of J_c in the YBCO/NTP samples at $H > H_m$, as shown in Fig. 4(a). Note that the J_c of the YBCO/NTP samples in Fig. 4(a) and hereafter are calculated using the effective cross-sectional area and H is applied along film normal. The effect of H on the J_c-t behavior of the YBCO/NTP films is further quantified in Fig. 4(b), in which most of the curves in Fig. 4(a) are replotted on a normalized scale [J_c/J_c (0.6 μm)]. For comparison, the inset of Fig. 4(b) shows the normalized J_c-t curves measured on the standard YBCO films. It can be seen that the J_c-t curve of the YBCO/NTP films gradually evolves into CP type with increasing H. At around 0.05–0.1 T, it shows a close resemblance to $J_c \propto t^{-1/2}$ indicated by the dash line, suggesting the dominance of the collective pinning by point defects as H is around $10H_m$. Note that this H range (0.05–0.1 T) is exactly where the two types of film show comparable J_c, also suggesting a similar pinning mechanism in this field range. With further increasing H, the effect of the TAFM becomes visible and more enhanced at higher H, which continuously weakens the J_c-t of the YBCO/NTP samples in a similar way as in the case of the standard YBCO samples shown in the inset. This complex effect of H on J_c-t indicates the existence of dual pinning systems in the YBCO/NTP films and suggests that higher density straight NTPs are necessary to extend a flat J_c-t to higher H fields.

In summary, we have fabricated YBCO/NTP films and studied their J_c-t behavior at 77 K and various magnetic fields of up to 5 T. Since the NTPs are linear defects aligned along the normal of the film and through nearly entire film thickness, they provide an enhanced pinning force F_p on each vortex, which remains constant at variable thickness. The enhanced pinning by NTPs results in high J_c values and effectively suppresses the TAFM. In addition, the t dependence of J_c observed in the standard YBCO films is much reduced in the YBCO/NTP samples at $H < H_m$ and may be completely eliminated when the NTPs' lateral dimension is made constant. Interestingly, the CP-type J_c-t behavior is resumed in YBCO/NTP samples $H \gg H_m$, which suggests a switch from the stronger NTP pinning to weaker pinning by randomly distributed point defects.

The authors acknowledge the supports from NSF and US-AFOSR.

*xiangw@ku.edu

[1] S. R. Flotyn, P. Tiwari, R. C. Dye, M. Q. Le, and X. D. Wu, Appl. Phys. Lett. **63**, 1848 (1993).
[2] S. R. Foltyn, Q. X. Jia, P. N. Arendt, L. Kinder, Y. Fan, and J. F. Smith, Appl. Phys. Lett. **75**, 3692 (1999).
[3] B. W. Kang, A. Goyal, D. R. Lee, J. E. Mathis, E. D. Specht, P. M. Martin, D. M. Kroeger, M. Paranthaman, and S. Sathyamurthy, J. Mater. Res. **17**, 1750 (2002).
[4] Q. X. Jia, H. Wang, Y. Lin, Y. Li, C. Wetteland, G. W. Brown, M. Hawley, B. Maiorov, S. R. Foltyn, L. Civale, P. N. Arendt, and J. L. MacManus-Driscoll, IEEE Trans. Appl. Supercond. **17**, 3243 (2007).
[5] A. Gurevich, MURI Program Review, 2005 (unpublished).
[6] A. I. Larkin and Yu. Ovchinnikov, J. Low Temp. Phys. **21**, 409 (1979).
[7] G. Blatter, M. V. Feigel'man, V. B. Geshkenbein, A. I. Larkin, and V. M. Vinokur, Rev. Mod. Phys. **66**, 1125 (1994).
[8] A. Catana, R. F. Broom, J. G. Bednorz, J. Mannhart, and D. G. Schlom, Appl. Phys. Lett. **60**, 1016 (1992).
[9] C. J. van der Beek, M. Konczykowski, A. Abaloshev, I. Abalo-

sheva, P. Gierlowski, S. J. Lewandowski, M. V. Indenbom, and S. Barbanera, Phys. Rev. B **66**, 024523 (2002).
[10] X. Wang and J. Z. Wu, Phys. Rev. B **76**, 184508 (2007).
[11] A. Gurevich, Supercond. Sci. Technol. **20**, S1 (2007).
[12] X. Wang and J. Z. Wu, Appl. Phys. Lett. **88**, 062513 (2006).
[13] S. R. Foltyn, H. Wang, L. Civale, B. Maiorov, Y. Li, M. P. Maley, and J. L. MacManus-Driscoll, Appl. Phys. Lett. **87**, 162505 (2005).
[14] T. L. Hylton and M. R. Beasley, Phys. Rev. B **41**, 11669 (1990).
[15] S. R. Foltyn, L. Civale, J. L. Macmanus-Driscoll, Q. X. Jia, B. Maiorov, H. Wang, and M. Maley, Nat. Mater. **6**, 631 (2007).
[16] G. W. Xu and J. Z. Wu (unpublished).
[17] R. L. S. Emergo, J. Z. Wu, T. J. Haugan, and P. N. Barnes (unpublished).
[18] A. O. Ijaduola, J. R. Thompson, R. Feenstra, D. K. Christen, A. A. Gapud, and X. Song, Phys. Rev. B **73**, 134502 (2006).
[19] M. Tinkham, *Introduction to Superconductivity*, 2nd ed. (McGraw-Hill, New York, 1996).